

MedChemComm

Accepted Manuscript



This is an *Accepted Manuscript*, which has been through the Royal Society of Chemistry peer review process and has been accepted for publication.

Accepted Manuscripts are published online shortly after acceptance, before technical editing, formatting and proof reading. Using this free service, authors can make their results available to the community, in citable form, before we publish the edited article. We will replace this *Accepted Manuscript* with the edited and formatted *Advance Article* as soon as it is available.

You can find more information about *Accepted Manuscripts* in the [Information for Authors](#).

Please note that technical editing may introduce minor changes to the text and/or graphics, which may alter content. The journal's standard [Terms & Conditions](#) and the [Ethical guidelines](#) still apply. In no event shall the Royal Society of Chemistry be held responsible for any errors or omissions in this *Accepted Manuscript* or any consequences arising from the use of any information it contains.



Journal Name

COMMUNICATION

Development of Subnanomolar Radiofluorinated (2-Pyrrolidin-1-yl)imidazo[1,2-*b*]pyridazine pan-Trk Inhibitors as Candidate PET Imaging Probes

Received 00th January 20xx,
Accepted 00th January 20xx

DOI: 10.1039/x0xx00000x

www.rsc.org/

Vadim Bernard-Gauthier^{a*}, Justin J. Bailey^a, Arturo Aliaga^b, Alexey Kostikov^c, Pedro Rosa-Neto^b, Melinda Wuest^a, Garrett M. Brodeur^d, Frank, Wuest^a, Ralf Schirmmacher^{a*}

Dysregulation of tropomyosin receptor kinases (TrkA/B/C) expression and signalling is recognized as a hallmark of numerous neurodegenerative diseases including Parkinson's, Huntington's and Alzheimer's disease. TrkA/B/C is known to drive tumorigenesis and metastatic potential in a wide range of neurogenic and non-neurogenic human cancers. The development of suitable positron emission tomography (PET) radioligands would allow an in vivo exploration of this versatile potential therapeutic target. Herein, the rational remodeling of the amide moiety of a 6-(2-(3-fluorophenyl)pyrrolidin-1-yl)imidazo[1,2-*b*]pyridazine-3-amide lead structure to accommodate efficient fluorine-18 labeling led to the identification of a series of fluorinated Trk inhibitors with picomolar IC₅₀. The ensuing representative radiolabeled inhibitors [¹⁸F]**16** ([¹⁸F]-(\pm)-IPMICF6) and [¹⁸F]**27** ([¹⁸F]-(\pm)-IPMICF10) constitute novel lead radioligands with about 2- to 3-orders of magnitude increased TrkB/C potencies compared to previous lead tracers and display favorable selectivity profiles and physicochemical parameters for translation into in vivo PET imaging agents.

INTRODUCTION

The tropomyosin receptor kinase (Trk) family consists of three structurally analogous tyrosine kinases with pivotal significance in the embryonic development and post-natal maintenance of the mammalian nervous system. Upon extracellular binding of cognate specific neurotrophins and subsequent kinase domain autophosphorylation of the full length receptors, the Trk/neurotrophin protein interplay activates key signal transduction pathways including Ras/MAPK, PI3K and PLC γ which spatiotemporally support growth, survival and differentiation within distinct neuronal populations.¹⁻³ Nerve growth factor (NGF) specifically interacts with TrkA, while brain derived neurotrophic factor (BDNF) and neurotrophin-3 (NT-3) selectively bind TrkB and TrkC respectively ($K_d \approx 1.7\text{-}2.3 \times 10^{-11}$ M).⁴ NT-3 was also shown to activate TrkA and TrkB, albeit with lower efficiency.⁴ TrkA receptor expression in the central nervous system (CNS) is mostly circumscribed to cholinergic neurons of the basal forebrain (BFCNs) and dorsal root ganglion (DRG).⁵⁻⁷ TrkA density is reduced in BFCNs

and cholinergic projections in the cerebral cortex at early Alzheimer's disease (AD) stages underlining the involvement of TrkA in the cognitive decline characteristic of the early onset of AD.^{8,9} In the periphery, TrkA activation is involved in nociception and is a validated target for chronic pain.¹⁰ In contrast to TrkA, TrkB/C have comparatively high expression levels in the CNS with topographies encompassing most brain regions including cortex, striatum, thalamus and cerebellum.¹¹⁻¹³ In rodents, the NTRK2 (TrkB) family gene expression includes the full length TrkB.tk+ (herein referred to as TrkB) and the truncated splice variants TrkB.T1 and TrkB.T2 which lack the intracellular kinase domain.^{14,15} TrkB.T1 has been characterized and shown to be abundantly expressed in the CNS.¹⁶ Specific biological functions of TrkB.T1 remain elusive but include negative regulation of TrkB.tk+ signalling and BDNF sequestration and translocation.¹⁷ The expression ratio of TrkB.tk+/TrkB.T1 are highly regulated in the embryonic and early postnatal nervous system development. In adult life, mounting evidences support TrkB isoform dysregulation and aberrant TrkB/BDNF signalling as a hallmark of neurodegenerative and psychiatric diseases/conditions including AD, Parkinson's disease (PD), Huntington's disease (HD), schizophrenia and traumatic brain injury (TBI).¹⁸⁻²²

Though historically explored in the context of neurology, Trk involvement in tumorigenesis and aggressiveness of human cancers is also well recognized.^{23,24} Indeed, the prototypical NTRK1 (TrkA) gene was initially identified from a colon carcinoma leading to a constitutively activated fused tropomyosin-TrkA protein.²⁵ Besides rearranged/mutated NTRK gene products, compelling evidence shows that overexpression of the intact Trk proto-oncoproteins, especially TrkB, is associated with aggressive tumor growth and treatment resistance in a set of neurogenic and non-

^a Department of Oncology, University of Alberta, 11560 University Avenue, Edmonton, AB, Canada, T6G 1Z2.

^b Translational Neuroimaging Laboratory, McGill Centre for Studies in Aging, Douglas Mental Health University Institute, 6875 Boulevard LaSalle, Montreal, QC, Canada, H4H 1R3.

^c McConnell Brain Imaging Centre, Montreal Neurological Institute, McGill University, 3801 University Street, Montreal, QC, Canada, H3A 2B4.

^d Oncology Research, The Children's Hospital of Philadelphia, 3501 Civic Center Blvd., Philadelphia, PA, USA, 19104-4302.

† Electronic Supplementary Information (ESI) available: [Experimental procedures, supplementary figures, tables, scheme, crystallographic data, radio-HPLC chromatograms, and ¹H, ¹³C NMR spectral data]. See DOI: 10.1039/x0xx00000x

Journal Name

COMMUNICATION

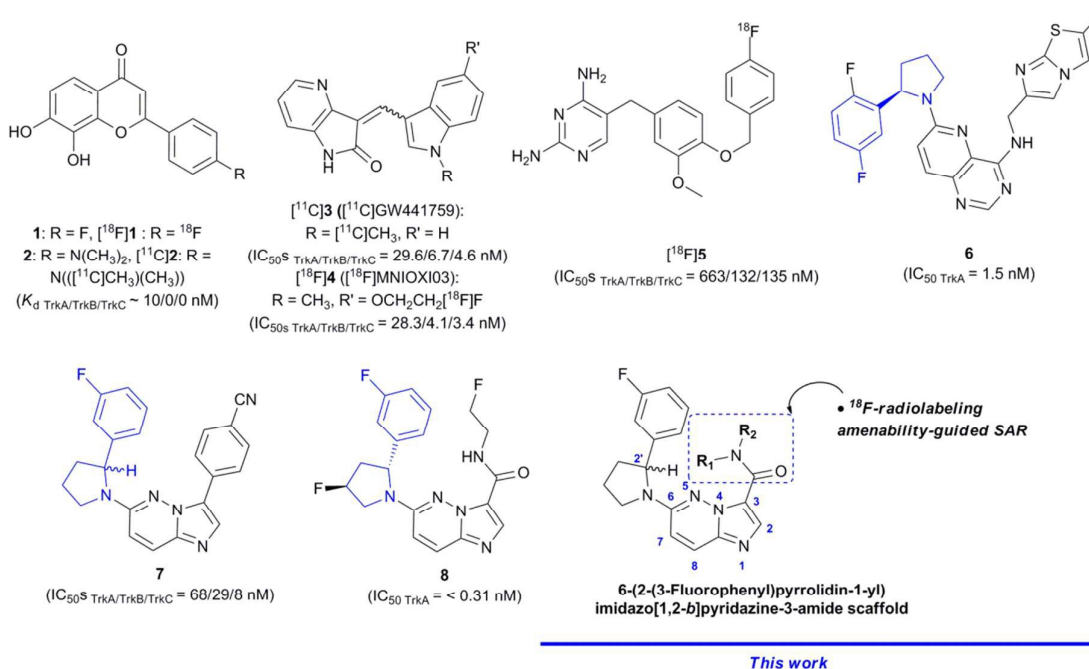


Fig.1 Structure of Trk agonistic radioligands, tyrosine kinase inhibitor (TKIs) radioligands and fluorophenyl- and difluorophenyl pyrrolidine-containing Trk TKIs.

neurogenic neoplasms including neuroblastoma and pancreatic cancer.^{26,27} During the last decade, considerable medicinal chemistry effort, mostly focused towards intracellular binding kinase inhibitors, has led to the identification of diverse and highly potent selective pan-Trk tyrosine kinase inhibitors (TKIs) as putative cancer therapeutics.^{28–31}

In order to non-invasively assess and monitor TrkA/B/C levels in the brain and in cancer, our group has sought to develop carbon-11 and ^{18}F -labeled Trk-targeted positron emission tomography (PET) radiotracers suitable for in vivo imaging. We have previously described both extracellular and intracellular binding PET radioligands, the first of which being the TrkB selective 7,8-dihydroxyflavone-based probes [^{18}F]**1** and [^{11}C]**2** (Figure 1).³² These radioligands, based on one of the rare efficacious small molecules to bind the extracellular Trk proteins described thus far suffered extensive metabolism in vivo and did not permeate the blood brain barrier (BBB) despite favorable in vitro profiling. More recently, we reported on the development of low nanomolar pan-Trk inhibitor [^{11}C]GW441759 and an analogous fluorinated derivative [^{18}F]**4**.³³ Preclinical imaging in rodents confirmed [^{11}C]GW441759 as the first brain penetrating Trk PET radiotracer but blocking studies failed to demonstrate specific brain binding at the tested dose. Both [^{11}C]GW441759 and [^{18}F]**4** also successfully imaged Trk in rat brain sections and human neuroblastoma tumor samples expressing TrkB

in vitro. In addition, the radiosynthetic methodology to access the fluorinated demethoxy derivative of the Trk inhibitor GW2580 ([^{18}F]**5**), was described.³⁴ Despite its unique selectivity, [^{18}F]**5** only displays moderate potencies towards Trk ($\text{IC}_{50}^{\text{S}}$ = 135–663 nM) and lacks necessary physicochemical properties to be suitable for brain PET imaging (Figure 1). Those radioligands are currently being evaluated for peripheral neuroblastoma tumor imaging by our group. As far as Trk neuroimaging is concerned, it would be desirable to concentrate efforts on compounds exhibiting subnanomolar affinities for Trk in combination with desired properties for PET ligand development (including $B_{\text{max}}/K_d > 10$, $\text{cLogD}_{7.4}$ in the range of 2.0–3.5, topological polar surface area (TSPA) < 80 Å², hydrogen bond donor (HBD) ≤ 1).³⁵ Amenability to fluorine-18 labeling ($t_{1/2} = 109.8$ min; 97% β^+ ; $E_{\text{max}}(\beta^+) = 0.64$ MeV) would also be favorable due to the better nuclear properties, including longer half-life which allow for longer synthesis time and shipping, as compared to carbon-11.

In recent years, diverse scaffolds including heterocycle cores such as imidazo[1,2-b]pyridazine, pyrido[3,2-d]pyrimidine and pyrazolo[1,5-a]pyrimidine related through conserved fluorinated 2-phenylpyrrolidines fragments have emerged as Trk-selective inhibitor pharmacophores (**6–8**, Figure 1).^{36–43} (*R*)-2-phenylpyrrolidine is the preferred enantiomeric building block. However in most cases where pure (*S*)-2-phenylpyrrolidine

containing derivatives were characterized, nanomolar Trk inhibitions were still achieved.³⁷ Moreover, *N*-(2-fluoroethyl)acetamide inhibitor (*R*)-**8** and related compounds showed unprecedented picomolar potencies towards TrkA.³⁷ Very recently, a derivative of **7** was also shown to achieve tumor regression in a KM12 rat tumor model.⁴² We hypothesized that a scaffold derived from compound **8**, which provides a favorable alignment of the required physicochemical parameters for PET radioligand development and was shown to tolerate numerous 3-carboxamide structural alterations, would be valuable in the exploration of new Trk radioligands bearing purposely designed ¹⁸F-radiolabeled amide substituents. Herein, we present the design, syntheses and first in vitro evaluation of novel ¹⁸F-labeled Trk PET 6-(2-(3-fluorophenyl)pyrrolidin-1-yl)imidazo[1,2-*b*]pyridazine-3-amide radioligand candidates.

RESULTS AND DISCUSSION

A priority of this work was to explore and identify the optimal fluorinated 3-carboxamide building blocks integrated into the (2-pyrrolidin-1-yl)imidazo[1,2-*b*]pyridazine lead structure to yield Trk inhibitors of highest possible affinity. As another important premise, the identified compounds should be easily labeled in one step with [¹⁸F]fluoride to facilitate applicability. Since both (*R*)- and (*S*)-substituted pyrrolidines were previously shown to be highly potent and the racemic building block is readily available, we selected the racemic 2-(3-fluorophenyl)pyrrolidine motif with the core structure of lead **8** as a starting point in our structure activity relationship (SAR) study.⁴⁴ Following procedures previously described,⁴¹ this approach allowed the preparation of a sufficient amount of the key 3-carboxylic acid intermediate **9** for further derivatization (Table 1, see Scheme S1; supporting information).

Amide Moiety Design for Radiolabeling and Chemistry

It was noted that despite the excellent potency attained with the *N*-(2-fluoroethyl)-amide substituent in **8** as reported in patent literature, the synthesis of the ¹⁸F-labeled counterpart of this motif would require a multistep approach using 2-[¹⁸F]-fluoroethylamine which in turn would ultimately limit the later use of the resulting radioligand in a clinical setting.⁴⁵ Initial SAR efforts therefore focussed on introducing small aliphatic fluorinated chains attainable as ¹⁸F-isotopologues via simple *S_N2*-type radiofluorination but which would not undergo intramolecular five-*Exo-Tet* cyclisation to the oxazoline upon prior functionalization with a leaving group or during the radiolabeling. In this context structurally analogous fluorocyclobutyl moieties were selected. Previous reports also suggest that ¹⁸F-labeled fluorocyclobutyl-containing PET probes may be metabolically more robust than their linear equivalents.⁴⁶ Hence, compounds **15** and **16** along with the linear *N*-fluoroalkyl amides **13** and **14** were synthesized in good yield via HATU coupling between **9** and the corresponding amines (Table 1). In order to assess the impact of the amide proton towards Trk binding, the 3-azetidine amide **17** was synthesized as the closest cyclized structural analog to **13**. Direct amidation of the ester intermediate **10** also efficiently provided the simpler derivatives **11** and **12**.

Using docking simulations, congruent binding poses to TrkA/B/C were initially obtained in both the inactive (DFG-out) and active (DFG-in) conformations for **16** (*R* and *S*; Figures S1,S2; supporting information). Choi et al.⁴² recently described X-ray cocrystal structures of (*R*)-enantiomer derivatives of **7** bound to TrkA and

TrkC in DFG-in and DFG-out conformations and suggested that the favoured binding mode likely depends upon the substituent pattern of the imidazo[1,2-*b*]pyridazine core. The binding modes of **16** and derivatives thereof obtained in our in silico experiments corroborate those X-ray results with regard to the binding with the active Trk kinases. In this conformation, the N₁ from the imidazo[1,2-*b*]pyridazine interacts via H-bonding with the backbone nitrogen of Met592/636 (TrkA/TrkB) from the hinge and provides excellent overlap of the fluorophenyl ring to the ribose binding pocket including π -stacking with the proximal Phe521/565.^{47,48} In this model, the amide substituent is pointing towards the solvent region and rotation of the C₃-C(carbonyl) can lead to the amide carbonyl or NH directed at the hinge (Figure S1). The predicted binding pose of the representative compound **27** (*vide infra*) is shown in Figure 2.

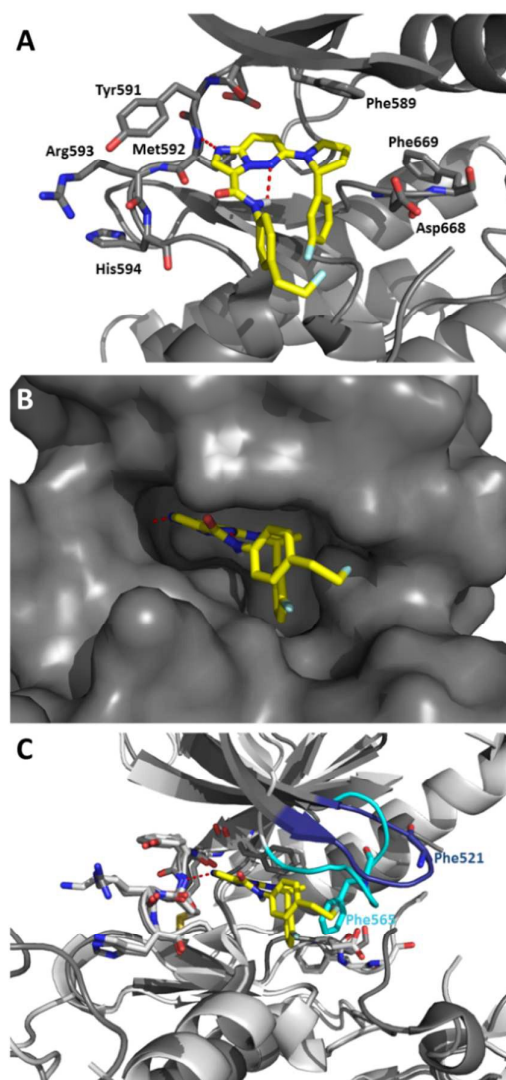
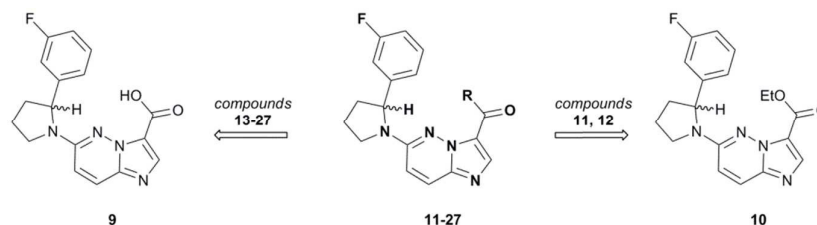


Fig. 2 Predicted binding poses for (*R*)-**27** bound to TrkA/B in DFG-in conformation. (A) Docking of (*R*)-**27** to the ATP binding site of TrkA (PDB 4PMT). (B) Surface model of (*R*)-**27** docked to TrkA (PDB 4PMT). (C) Superposition of TrkB (pale gray, DFG-in, PDB 4AT3) and the docking of (*R*)-**27** with TrkA (dark gray, PDB 4PMT). The TrkA (blue) and TrkB (cyan) glycine-rich loops are highlighted.

Journal Name

COMMUNICATION

Table 1 SAR and In Vitro Enzymatic Activities and Physicochemical Data for Imidazo[1,2-*b*]pyridazines Trk Inhibitors

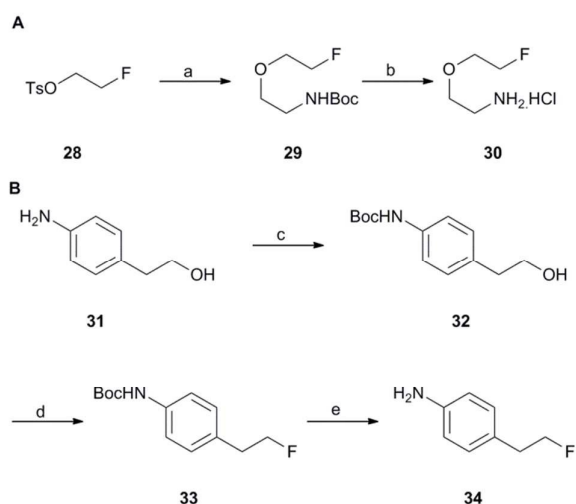
Cpd	R	clogP	TPSA (Å ²)	IC ₅₀ (nM) ^a			IC ₅₀ _{TrkA} /IC ₅₀ _{TrkB} ; IC ₅₀ _{TrkA} /IC ₅₀ _{TrkC}	B _{max} /IC ₅₀ (caudate putamen/cortex; ^b TrkA)	B _{max} /IC ₅₀ (whole brain average; TrkB/C) ^b
				TrkA	TrkB	TrkC			
10		2.39	59.73	17.7	2.36	1.37	7.5; 12.9	0.8/0.1	11.0
9		1.66	70.73	>10 000	3250	1880	- ^c	- ^c	- ^c
11		1.16	76.52	12.9	1.31	0.943	9.8; 13.7	1.1/0.2	19.8
12		1.51	62.53	7.66	0.565	0.374	13.6; 20.5	1.8/0.3	46.0
13 ^d		1.70	62.53	1.11 ± 0.13	0.037 ± 0.013	0.080 ± 0.030	30.0; 13.8	8.9/1.8	703
14 ^d		2.15	62.53	2.48 ± 0.96	0.105 ± 0.043	0.115 ± 0.034	23.6; 21.6	4.0/0.8	248
15 ^d		2.28	62.53	2.69 ± 0.24	0.120 ± 0.021	0.163 ± 0.011	22.4; 16.5	3.7/0.7	217
16 ^d		2.08	62.53	1.91 ± 0.41	0.076 ± 0.035	0.076 ± 0.035	25.1; 25.1	5.2/1.0	342
17		1.93	53.74	140	22.8	13.8	6.1; 10.1	0.1/0.01	1.1
18		3.06	62.53	1.50	0.132	0.154	11.4; 9.7	9.1/1.3	197
19		1.45	71.76	4.31	0.926	0.440	4.7; 9.8	3.2/0.5	28.1
20		2.88	62.53	3.53	1.09	0.580	3.2; 6.1	3.9/0.6	23.8
21		2.88	62.53	2.76	0.509	0.299	5.4; 9.2	4.9/0.7	51.1
22		2.91	71.76	11.2	1.96	0.950	5.7; 11.8	1.2/0.2	13.3

Journal Name

COMMUNICATION

23		3.17	62.53	5.00	0.584	0.408	8.6; 12.3	2.7/0.4	44.5
24		3.1	71.76	4.80	0.456	0.233	10.5; 20.6	2.8/0.4	57.0
25^d		3.17	62.53	2.06 ± 0.17	0.131 ± 0.047	0.214 ± 0.093	15.7; 9.6	4.8/1.0	199
26^d		3.17	62.53	1.94 ± 0.90	0.080 ± 0.012	0.095 ± 0.013	24.3; 20.4	5.1/1.0	325
27^d		3.61	62.53	2.10 ± 0.34	0.099 ± 0.008	0.127 ± 0.005	21.2; 16.5	4.7/1.0	262

^a [γ -³³P]ATP-based enzymatic assay performed by Reaction Biology. ^b Calculated with B_{\max} value for the caudate putamen for TrkA and from the whole brain for TrkB from Ref. 55 and the IC_{50} s from TrkA and TrkB respectively. ^c Not determined. ^d Values accompanied by standard deviation were averaged from three independent experiments.



Scheme 1 Reagents and conditions: (A) (a) *N*-boc-ethanolamine, NaH, DMF, rt, 12 h (50%). (b) TFA, CH₂Cl₂, rt, 1 h, then HCl (1M in diethyl ether) (98%). (B) (c) Boc₂O, Et₃N, THF, 0°C - rt, 16 h (85%). (d) DAST, CH₂Cl₂, -78°C, 30 min then 0°C, 6 h (86%). (e) TFA, CH₂Cl₂, 0°C - rt, 5 h (93%).

With the carbonyl pointing outward, additional water-mediated H-bonds to residue Met592/636 may occur while a strong intramolecular H-bond is possible between the amide proton and N₅. It is likely that the binding of this preorganized rigidified low energy conformation to Trk in the DFG-in mode explains in part the increased potencies observed between inhibitors such as **8** versus **7** due to a lower entropic penalty. This binding conformation is also consistent with the disclosure of highly potent related macrocyclized Trk inhibitors.⁴⁹

In agreement with the plausible binding mode elucidated, the synthesis of potential inhibitors incorporating larger amide substituents was undertaken. Compounds bearing a 4,4-difluorocyclohexyl group and a *N*-2-(2-fluoroethoxy)ethyl chain were synthesized. The amine **30** required for the synthesis of **19** was obtained in two steps from 2-fluoroethyl 4-methylbenzenesulfonate **28** (Scheme 1A). Fluorobenzyl- (**20-22**) and fluorophenylamide (**23-27**) compounds were also obtained. The

required aniline **34** for the synthesis of **27** was prepared via a protection/DAST fluorination/deprotection sequence (Scheme 1B). It was anticipated that compounds **20-26** would be accessible for radiolabeling using direct radiofluorination of non-activated arenes bearing iodonium ylides leaving groups if required.^{50,51} Compound **27** was designed to be readily accessible using conventional S_N2 radiofluorination. Compounds **22** and **26** also bear alternative anisole moieties suitable for carbon-11 labeling using [¹¹C]CH₃I. The suggested low energy intramolecular H-bonded U-shaped conformation was illustrated by single crystal X-ray diffraction of the representative compound (*R*)-**22** (obtained from the racemate; Figure 3).

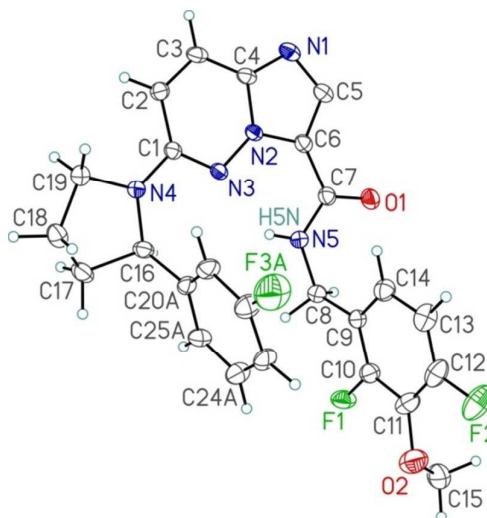


Fig. 3 Single-crystal X-Ray structure of (*R*)-**22**; ellipsoids drawn at 30% probability.

In Vitro Binding Studies

The inhibitory activity of compounds **9-27** was obtained using a [γ -³³P]ATP-based enzymatic assay.⁵² The TrkA/B/C assay data is summarized in Table 1. The most potent inhibitor for all Trk proteins was derivative **13** containing the 2-fluoroethyl amide lateral chain with an IC_{50} of 1.11 nM for TrkA, 0.037 nM for TrkB and 0.080 nM for TrkC. To our satisfaction, replacement of the linear

chain of **13** with the fluorocyclobutyl found in **16** did not significantly alter the excellent potencies observed (1.05 to 2.05-fold reduction). Elongation of the amide chains in **14** and **15** by one additional carbon only slightly affected the potencies. Compound **12** displayed subnanomolar and low nanomolar potencies for TrkB/C and TrkA respectively while being ~2-fold more potent than the primary amide **11** for all Trks. While the ester **10** displayed significantly lower, yet still low nanomolar potencies, the presence of a carboxylate in **9** was highly detrimental to the affinity. As predicted above, the removal of the amide proton in **17** had a negative effect despite this inhibitor being the closest analog of **13** with respect to all other structural elements (616-fold decreased potency for TrkB). As expected, good tolerance of the sterically demanding gem-difluorocyclohexane (compound **18**), extended linear chain (compound **19**) and aryl-containing derivatives (compounds **20-27**) was also observed. The best potencies in the aryl-containing derivatives were attained by fluorophenyl-compared to fluorobenzylamides. Inhibitors **13** and **16** were found to match the Trk activity of staurosporine – to our knowledge, the most potent Trk inhibitor currently available (Figure S20). All compounds also show favorable clogP and TPSA values for translation into PET tracers (Table 1).

Overall, we identified a total of 8 inhibitors (**13-16**, **18**, **25-27**) displaying approximately 200 pM potencies or lower for TrkB/C and low nanomolar potencies for TrkA with radiotracer-favorable properties. These most potent derivatives, except for **18**, were also found to display the best selectivity profile in the assayed conditions (TrkB/C versus TrkA, Figure S21).⁵³ Due to the extensive sequence conservation in the 40 residues likely to be involved in binding at the ATP site (DFG-in) between TrkA and TrkB (95%) and TrkB and TrkC (100%), it is largely accepted that Trk isoform selectivity for ATP competitive inhibitors will be challenging to attain.^{28,48} The observed moderate selectivity here may be related to the organization of the glycine-rich loops (Figure 2C) or the difference in conformational restriction of the hinge in TrkA versus TrkB as previously suggested.⁴⁸ While the development of a pan-Trk PET radioligand would be highly valuable, selectively imaging TrkB/C independently of TrkA and vice versa would be even more desirable. In imaging studies, the specific PET signal is contingent on both the receptor density (B_{\max}) and affinity of the tracer for the specific target.⁵⁴ Hence, for Trk neuroimaging, visualizing TrkB/C selectively will likely be facilitated by the drastic differences in B_{\max} and topographies of Trks in the brain. Binding studies with [¹²⁵I]-neurotrophins along with in situ hybridization experiments have shown that TrkB/C densities largely exceed that of TrkA.^{7,13,55} While TrkB/C are largely co-expressed in all brain regions with an average $B_{\max} > 26$ nM, TrkA expression is mostly restricted to the striatum with a $B_{\max} < 9$ nM. Therefore, the (TrkB/C)/TrkA B_{\max} ratios for all brain regions range from 3 in the striatum to $\gg 10$ in most other brain regions. It should then be expected that, even in the absence of selectivity, the binding of a PET radiolabeled Trk inhibitor should mostly reflect the TrkB/C distribution. This implies that selective visualization of TrkA in the brain would require a highly selective probe to overcome those B_{\max} differences. With our most potent and selective compounds (**13-16**, **18**, **25-27**), using IC_{50} values as a substitute for K_d , this translates into substantial whole brain average binding potentials for TrkB/C and significantly lower values for TrkA (striatum; Table 1).

Compounds **16** and **27** were selected for initial evaluation based on their potencies and expected labeling in one step. The selectivity profile of the two inhibitors was first performed in the presence of 0.1 μ M of compounds on a panel of 20 kinases (Table 2). This initial

off-Trk kinase coverage included targets from different kinase groups with an emphasis on kinases expressed in the nervous system and neoplasms. Only ERBB2/HER2 and EGFR were significantly affected by co-incubation of **16** with remaining activities of 50% and 67% respectively. Those interactions were less pronounced in the presence of **27**. Other minor reductions in inhibitory activity were observed with **16** towards FLT3 and PDHK1 (15% reduction) and **27** with PDHK1 (20% reduction). Overall both compounds were found to be ≥ 1000 -fold selective for TrkB/C for all tested kinases.

Table 2 Kinase Profiling of **16** and **27**

Kinase Target	Inhibitory activity of 16 (% remaining at 0.1 μ M \pm SD) ^a	Inhibitory activity of 27 (% remaining at 0.1 μ M \pm SD) ^a
CSF-1R	102.53 \pm 0.91	104.90 \pm 3.63
VEGRR-2	110.00 \pm 0.54	95.05 \pm 0.79
ITK	93.38 \pm 0.22	97.63 \pm 0.80
FLT3	85.07 \pm 0.11	95.09 \pm 1.39
ERK1/MAPK3	103.41 \pm 0.08	101.28 \pm 0.40
ABL1	95.64 \pm 0.46	91.34 \pm 0.64
c-Src	97.01 \pm 0.52	103.11 \pm 0.40
EGFR	66.65 \pm 2.02	93.12 \pm 4.80
c-MET	94.81 \pm 1.41	97.05 \pm 1.78
P38A/MAPK14	98.46 \pm 1.58	99.54 \pm 0.07
ALK	95.20 \pm 0.92	89.00 \pm 0.57
ERBB2/HER2	49.61 \pm 0.55	79.63 \pm 0.13
JNK1	99.44 \pm 0.08	100.24 \pm 6.2
PDHK1	85.47 \pm 0.13	78.90 \pm 0.26
PDGFRA	99.81 \pm 1.14	99.52 \pm 0.05
JAK1	90.67 \pm 0.42	99.69 \pm 1.43
SYK	105.04 \pm 0.28	103.93 \pm 0.59
RET	90.21 \pm 1.10	105.87 \pm 0.06
BRAF	100.30 \pm 1.48	94.07 \pm 1.97
c-KIT	104.76 \pm 0.57	100.86 \pm 0.48
TrkA	2.95 \pm 0.46 ^b	3.37 \pm 0.65
TrkB	0.44 \pm 0.29 ^b	0.56 \pm 0.18
TrkC	0.39 \pm 0.52 ^b	0.58 \pm 0.40

^a [γ -³³P]ATP-based enzymatic assay performed by Reaction Biology. Values relative to DMSO controls; duplicate experiments. ^b Derived from dose-response curves at 1.11x10⁻⁰⁷ M (triplicates).

Radiosyntheses and Plasma Stability

Radiosyntheses of [¹⁸F]**16** (named [¹⁸F]IPMICF6) and [¹⁸F]**27** (named [¹⁸F]IPMICF10) proceeded from the corresponding tosylate precursors. Precursor **36** was obtained in 70% yield from the intermediate **35** which was synthesized near-quantitatively from the coupling of **9** with 3-aminocyclobutanol.HCl (Scheme 2). Synthesis of the tosylate **41** was obtained in 45% overall yield and 4 steps from 2-(4-aminophenyl)ethanol (**37**, Scheme 3). Initial ¹⁸F-fluoride incorporation was optimized manually using standard conditions. The radiosynthesis of [¹⁸F]**16** proceeded efficiently at 120°C for 10 min in anhydrous dimethylformamide (DMF) with ¹⁸F-fluoride as a Kryptofix-222/K⁺/[¹⁸F]F⁻ complex while the ideal conditions to obtain [¹⁸F]**27** required a lower temperature due to the apparent degradation of the tosylate precursor. Following semi-

high affinity binding sites of [125 I]BDNF, [125 I]NT3 and [125 I]NT4/5 and the topographies of TrkB and TrkC mRNA hybridization (including cortex, striatum, thalamus and cerebellum; Figure 4).¹³ In those assays, moderate but significant specific binding was confirmed with co-incubation of non-labeled **16** (1.0 μ M; $\Delta \sim -30\%$) and similar blocking results were also obtained with the incubation of [18 F]**27** in the presence of the selective Trk inhibitor GNF-5837 (Figure S22). The analogous blocking obtained with the racemic **16** and the structurally unrelated oxindole-based DFG-out inhibitor GNF-5837 is indicative that both the (*R*)- and (*S*)-enantiomers binds Trk receptors in vitro.

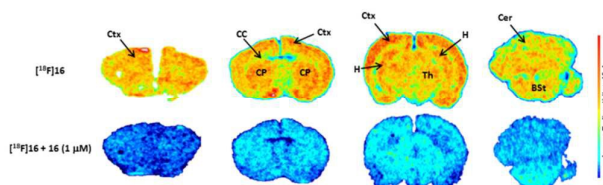


Fig. 4 Representative in vitro autoradiograms from coronal sections of rat brain showing the binding of [18 F]**16** and competition experiments with **16** (1 μ M) (successive sections between baseline and blocking; anterior: left, posterior: right). BSt = brain stem; CC = corpus callosum; Cer = cerebellum; CP = caudate putamen; Ctx = cortex; H = hippocampus; Th = Thalamus.

CONCLUSION

In this study we report the design, synthesis and evaluation of a series of novel fluorinated 6-(2-(3-fluorophenyl)pyrrolidin-1-yl)imidazo[1,2-b]pyridazine-based Trk inhibitors with the aim of identifying suitable candidates for translation into PET imaging agents for brain and tumor imaging. Compounds **16** and **27** were selected from a group of 8 identified structures which displayed around or <200 pM potency against TrkB/C and were shown to be at least 1000-fold selective in a kinase panel. The rationally designed amide side chains of **16** and **27** allowed for their straightforward 18 F-radiolabeling. In vitro autoradiography using [18 F]**16** and [18 F]**27** on coronal rat brain sections confirmed specific binding to TrkB/C-rich brain regions. The selected representative probes from this series, [18 F]**16** ([18 F]IPMICF6) and [18 F]**27** ([18 F]IPMICF10), constitute novel potential PET tracers with 2 to 3 orders of magnitude potency improvement compared with our previous leads [11 C]GW441759 and [18 F]**5**, while possessing various other key properties suitable for conversion into PET tracers. While the radioligands developed in this work were evaluated as isomeric mixtures, further structural refinement is currently ongoing in order to deliver pure pyrrolidine motifs as it is to be expected that those different enantiomers will also display distinct affinities and potentially distinctive in vivo imaging profiles. Comparative in vivo imaging studies of [18 F]**16**, [18 F]**27** and other radiotracers derived from this work will be reported in due course.

Acknowledgement

We thank Dr. Esther Schirmacher for reading the manuscript and providing useful comments. We are thankful to Angelina Morales-Izquierdo for the mass spectrometry analysis. We thank Marilyn Grand'Maison for the valuable help for the preparation of figures. We are also grateful to Dave Clendering and Blake Lazaruko from the Edmonton PET Centre and Robert Hopewell, Miriam Kovacevic and

Dean Jolly from the Montreal Neurological Institute for radionuclide production. We thank Bob McDonald and Michael Ferguson for the X-ray crystallographic service. This work was financially supported by Canada Foundation for Innovation (CFI) project no. 203639 to R.S.

Notes and references

- 1 E. J. Huang and L. F. Reichardt, *Annu. Rev. Neurosci.*, 2001, 24, 677-736.
- 2 E. J. Huang and L. F. Reichardt, *Annu. Rev. Neurosci.*, 2003, 26, 609-642.
- 3 M. V. Chao, *Nat. Rev. Neurosci.*, 2003, 4, 299-309.
- 4 M. Pattarawarapan and K. Burgess, *J. Med. Chem.*, 2003, 46, 5277-5291.
- 5 D. M. Holtzman, J. Kilbridge, Y. Li, E. T. Cunningham, N. J. Lenn, D. Clary, L. F. Reichardt and W. C. Mobley, *J. Neuroscience*, 1995, 15, 1567-1576.
- 6 Y. Muragaki, N. Timothy, S. Leight, B. L. Hempstead, M. V. Chao, J. Q. Trojanowski and V. M. Lee, *J. Comp. Neurol.*, 1995, 356, 387-397.
- 7 A. C. Altar, L. E. Burton, G. L. Bennett and M. Dugich-Djordjevic, *Proc. Natl. Acad. Sci.*, 1991, 88, 281-285.
- 8 (a) S. D. Ginsberg, S. Che, J. Wu, S. E. Counts and E. J. Mufson, *J. Neurochem.* 2006, 97, 475-487. (b) E. J. Mufson, J. M. Li, T. Sobreviela and J. H. Kordower, *Neuroreport*, 1996, 20, 25-29.
- 9 S. E. Counts, M. Nadeem, J. Wu, S. D. Ginsberg, H. U. Saragovi and E. J. Mufson, *Ann. Neurol.*, 2004, 56, 520-531.
- 10 (a) J. R. Ghilardi, K. T. Freeman, J. M. Jimenez-Andrade, W. G. Mantyh, A. P. Bloom, M. A. Kuskowski and P. W. Mantyh, *Mol Pain.*, 2010, 6, 87. (b) P. W. Mantyh, M. Koltzenburg, L. M. Mendell, L. Tive and D. L. Shelton, *Anesthesiology*, 2011, 115, 189-204.
- 11 Y. Muragaki, N. Timothy, S. Leight, B. L. Hempstead, M. V. Chao, J. Q. Trojanowski and V. M. Lee, *J. Comp. Neurol.*, 1995, 356, 387-397.
- 12 L. Tessarollo, P. Tsoulfas, D. Martin-Zanca, D. J. Gilbert, N. A. Jenkins, N. G. Copeland and L. F. Parada, *Development*, 1993, 118, 463-475.
- 13 C. A. Altar, J. A. Siuciak, P. Wright, N. Y. Ip, R. M. Lindsay and S. J. Wiegand, *Eur. J. Neurosci.*, 1994, 6, 1389-1405.
- 14 R. Klein, D. Conway, L. F. Parada and M. Barbacid, *Cell*, 1990, 61, 647-656.
- 15 D. S. Maddlemas, R. A. Lindberg and T. Hunter, *Mol Cell Biol*, 1991, 11, 143-153.
- 16 M. Silhol, F. Bonnichon, F. Rage and L. Tapia-Arancibia, *Neuroscience*, 2005, 132, 613-624.
- 17 B. M. Fenner, *Cytokine & Growth Factor Review*, 2012, 23, 15-24.

- 18 F. Zhang, Z. Kang, W. Li, Z. Xiao and X. Zhou, *J. Clin. Neurosci.*, 2012, 19, 946-949.
- 19 F. Fumagalli, G. Racagni and M. A. Riva, *Pharmacogenomics*, 2006, 6, 95-104.
- 20 S. Gines, M. Bosch, S. Marco, N. Gavalda, M. Diaz-Hernandez, J. J. Lucas, J. M. Canals and J. Alberch, *Eur. J. Neurosci.*, 2006, 23, 649-658.
- 21 A. Pillai, *Neurosignals.*, 2008, 16, 183-193.
- 22 G. S. Griesbach, D. A. Hovda and F. Gomez-Pinilla, *Brain Res.*, 2009, 1288, 105-115.
- 23 C. J. Thiele, Z. Li and A. E. McKee, A. E., *Clin. Cancer Res.*, 2009, 15, 5962-5967.
- 24 A. Nakagawara, *Cancer Lett.*, 2001, 107-1114.
- 25 D. Martin-Zanca, S. H. Hughes and M. A. Barbacid, *Nature*, 1986, 319, 743-748.
- 26 G. M. Brodeur, J. E. Minturn, R. Ho, A. M. Simpson, R. Iyer, C. R. Varela, J. E. Light, V. Kolla and A. E. Evans, *Clin. Cancer Res.*, 2009, 15, 3244-3250.
- 27 G. M. Scwab, S. Fujioka, C. Schmidt, Z. Li, W. A. I. Frederick, Y. Yang, K. Yokoi, D. B. Evans, J. L. Abbruzzese, K. R. Hess, W. Zhang, I. J. Fidler and P. J. Chiao, *Clin. Cancer Res.*, 2005, 11, 440-449.
- 28 (a) T. Wang, D. Yu and M. L. Lamb, *Expert Opin. Ther. Pat.*, 2009, 19, 305-319. (b) C. McCarthy and E. Walker, *Expert Opin. Ther. Pat.*, 2014, 24, 731-744.
- 29 P. Albaugh, Y. Fan, Y. Mi, F. Sun, F. Adrian, N. Li, Y. Jia, Y. Sarkisova, A. Kreuzsch, T. Hood, M. Lu, G. Liu, S. Huang, Z. Liu, J. Loren, T. Tuntland, D. S. Karanewsky, H. M. Seidel and V. Molteni, *ACS Med. Chem. Lett.*, 2012, 3, 140-145.
- 30 J. L. Croucher, R. Iyer, N. Li, V. Molteni, J. Loren, W. P. Gordon, T. Tuntland, B. Liu and G. M. Brodeur, *Cancer Chemother. Pharmacol.*, 2015, 75, 131-141.
- 31 A. E. Evans, K. D. Kisselbach, X. Liu, A. Eggert, N. Ikegaki, A. M. Camoratto, C. Dionne and G. M. Brodeur, *Med. Pediatr. Oncol.* 2001, 36, 181-184.
- 32 V. Bernard-Gauthier, M. Boudjemeline, P. Rosa-Neto, A. Thiel and R. Schirmacher, *Bioorg. Med. Chem.*, 2013, 21, 7816-7829.
- 33 V. Bernard-Gauthier, A. Aliaga, A. Aliaga, M. Boudjemeline, R. Hopewell, A. Kostikov, P. Rosa-Neto, A. Thiel and R. Schirmacher, *ACS Chem. Neurosci.*, 2015, 6, 260-276.
- 34 V. Bernard-Gauthier and R. Schirmacher, *Bioorg. Med. Chem. Lett.*, 2014, 24, 4784-4790.
- 35 L. Zhang, A. Villalobos, E. M. Beck, T. Bocan, T. A. Chappie, L. Chen, S. Grimwood, S. D. Heck, C. J. Helal, X. Hou, J. M. Humphrey, J. Lu, M. B. Skaddan, T. J. McCarthy, P. R. Verhoest, T. T. Wager and K. Zasadny, *J. Med. Chem.*, 2013, 56, 4568-4579.
- 36 S. W. Andrews, J. Haas, Y. Jiang and G. Zhang, G. WO/2010/033941; International application No. PCT/US2009/057726; March 25, 2010.
- 37 P. A. Albaugh, G. Chopiuk, Y. Fan, B. T. Flatt, J. Loren, V. Molteni and J. M. Smith, WO/2012/034091 A1; International application No. PCT/US2011/051108; September 9, 2011.
- 38 J. Haas, S. W. Andrews, Y. Jiang and G. Zhang, WO/2010/048314 A1; International application No. PCT/US2009/061519; April 29, 2010.
- 39 S. Allen, S.S. Andrew, K. R. Condroski, J.; Haas, L. Huang, L.; Jiang, T. Kercher and J. Seo, WO/2011/006074 A1; International application No. PCT/US2010/041538; January 11, 2011.
- 40 P. K. Sasmal, S. Ahmed, A. Tehim, V. Pradkar, P. Dattatreya and N. J. Mavinahalli, WO/2013/088256 A1; International application No. PCT/IB2012/003013; June 20, 2013.
- 41 Y. Fan, J. Loren, V. Molteni, P. A. Albaugh, G. Chopiuk, J. M. Smith and B. T. Flatt, US/2012/0065184 A1; International application No. PCT/US2012/026377; August 30, 2012.
- 42 H. S. Choi, P. V. Rucker, Z. Wang, Y. Fan, P. Albaugh, G. Chopiuk, F. Gessier, F. Sun, F. Adrian, G. Liu, T. Hood, N. Li, Y. Jia, J. Che, S. McCormack, A. Li, J. Li, A. Steffy, A. Culazzo, C. Tompkins, V. Phung, A. Kreuzsch, M. Lu, B. Hu, A. Chaudhary, M. Prashad, T. Tuntland, B. Liu, J. Harris, H. M. Seidel, J. Loren and V. Molteni, *ACS Med. Chem. Lett.*, 2015, 6, 562-567.
- 43 S. J. Stachel, J. M. Sanders, D. A. Henze, M. T. Rudd, H. P. Su, Y. Li, K. K. Nanda, M. S. Egbertson, P. J. Manley, K. L. Jones, E. J. Brnardic, A. Green, J. A. Grobler, B. Hanney, M. Leitl, M. T. Lai, V. Munshi, D. Murphy, K. Rickert, D. Riley, A. Krasowska-Zoladek, C. Daley, P. Zuck, S. A. Kane and M. T. Bilodeau, *J. Med. Chem.*, 2014, 57, 5800-5816.
- 44 It was decided that at a later stage, once the SAR study delineating the amide motif would be completed, selected radiolabeled inhibitors could then more easily be obtained in pure enantiomeric forms for comparison with the corresponding racemates. This decision was also motivated by the current worldwide sparteine shortage – the only described synthesis of the putatively preferred compound (R)-2-(3-fluorophenyl)pyrrolidine proceeding via a key sparteine-mediated lithiation stage (see ref. 38).
- 45 (a) C. Gilissen, G. Bormans, T. de Groot and A. Verbruggen, *J. Label Compd. Radiopharm.*, 1998, 41, 491-502. (b) M. Glaser, E. Arstad, A. Gaeta, J. Nairne, W. Tigg and E. G. Robins, *J. Label Compd. Radiopharm.*, 2012, 55, 326-331.
- 46 D. Franck, T. Knies, J. Steinbach, S. Zitzmann-Kolbe, M. Friebe, L. M. Dinkelborg and K. Graham, *Bioorg. Med. Chem.*, 2013, 21, 643-652.
- 47 No DFG-in TrkC crystal structure is publicly available.
- 48 T. Bertrand, M. Kothe, J. Liu, A. Dupuy, A. Rak, P. F. Berne, S. Davis, T. Gladysheva, C. Valtre, J. Y. Crenne and M. Mathieu, *J. Mol. Biol.*, 2012, 423, 439-453.
- 49 S. W. Andrews, K. R. Condroski, J. Haas, Y. Jiang, G. R. Kolakowski, J. Seo, H. Yang and Q. Zhao,

COMMUNICATION

Journal Name

WO/2011/146336 A1; International Application No. PCT/IB2012/003012; June 20, 2013.

- 50 J. Cardinale, J. Ermert, S. Humpert and H. H. Coenen, *RCS Adv.*, 2014, 4, 17293-17299.
- 51 B. H. Rotstein, N. A. Stephenson, N. Vasdev and S. H. Liang, *Nat. Comm.*, 2014, 5, 4365.
- 52 The assay was performed in using the same conditions than previously used in Ref. 33.
- 53 The use of the IC_{50} s obtained for TrkA/B/C comparison and selectivity is based on the hypothesis that K_{mATP} for TrkA, TrkB and TrkC do not differ significantly due to their conserved sequence at the ATP binding site.
- 54 L. M. Paterson, B. R. Kornum, D. J. Nutt, V. W. Pike and G. M. Knudsen, *Med. Res. Rev.*, 2013, 33, 54-111.
- 55 C. A. Altar, M. R. Criden, R. M. Lindsay and P. S. DiStefano, *J. Neurosci.*, 1993, 13, 733-743.